Dual-Solvent Li-Ion Solvation Enables High-Performance Li-Metal Batteries

Hansen Wang, Zhiao Yu, Xian Kong, William Huang, Zewen Zhang, David G. Mackanic, Xinyi Huang, Jian Qin, Zhenan Bao, and Yi Cui**

Novel electrolyte designs to further enhance the lithium (Li) metal battery cyclability are highly desirable. Here, fluorinated 1,6-dimethoxyhexane (FDMH) is designed and synthesized as the solvent molecule to promote electrolyte stability with its prolonged –CF_2– backbone. Meanwhile, 1,2-dimethoxyethane is used as a co-solvent to enable higher ionic conductivity and much reduced interfacial resistance. Combining the dual-solvent system with 1 M lithium bis(fluorosulfonyl)imide (LiFSI), high Li-metal Coulombic efficiency (99.5%) and oxidative stability (6 V) are achieved. Using this electrolyte, 20 μm Li||NMC batteries are able to retain ≈80% capacity after 250 cycles and Cu||NMC anode-free pouch cells last 120 cycles with 75% capacity retention under ≈2.1 μL mAh^{-1} lean electrolyte conditions. Such high performances are attributed to the anion-derived solid-electrolyte interphase, originating from the coordination of Li-ions to the highly stable FDMH and multiple anions in their solvation environments. This work demonstrates a new electrolyte design strategy that enables high-performance Li-metal batteries with multisolvent Li-ion solvation with rationally optimized molecular structure and ratio.

1. Introduction

Lithium (Li) metal is the ultimate anode choice for high energy battery systems due to its low electrode potential (−3.04 V vs standard hydrogen electrode) and high specific capacity (3860 mAh g^{-1}). However, implementations of practical Li-metal anodes are hindered by their poor cyclability.[1] The inevitable reaction between metallic Li and electrolytes causes the formation of chemically and mechanically fragile solid-electrolyte interphase (SEI). With the significant volume fluctuation during Li metal cycling, SEI easily cracks, leading to dendritic growth and accelerated Li corrosion, and raising safety concerns.[2,3] A variety of strategies have been proposed to address the issue including developments of artificial coatings[4–9] and designing of 3D porous frameworks as "hosts"[10–17] for Li metal. However, further improvements are still demanded to enable an energy-dense Li-metal battery with a practical cycle life.

Electrolyte engineering is a promising approach to enhance the Li-metal cyclability. Novel electrolyte formulations alter the Li-ion solvation environments,[18–21] enabling uniform Li deposition morphology, and improving SEI stability and cycling Coulombic efficiency (CE). Multiple design strategies have been reported, such as high concentration electrolytes (HCEs),[19,22] localized high concentration electrolytes (LHCEs),[23,24] dual-salt electrolytes,[25,26] all-fluorinated electrolytes,[27,28] and liquefied gas electrolytes.[29,30] Although these strategies enabled longer cycling Li-metal batteries, modifications to further improve cyclability and cost-efficiency are still needed. We recently demonstrated anode-free cells with high cycling performance based on 1 M lithium bis(fluorosulfonyl)imide (LiFSI) in the rationally designed fluorinated 1,4-dimethoxybutane (FDMB) solvent,[31] but its ionic and interfacial resistance requires further reduction. Therefore, new electrolyte designs that enable better rate capability without sacrificing cyclability are highly desired.

In this work, we design and synthesize 1,6-dimethoxyhexane (FDMH) that has longer -CF_2- backbone than FDMB, which shows further improved stability while maintaining the capability to solvate Li-ions. 1,2-dimethoxyethane (DME) is used as a co-solvent with an optimized ratio (ν_{FDMH}:ν_{DME} = 6:1) to effectively reduce ionic and interfacial resistance without compromising electrolyte stability. With this 1 M LiFSI/6FDMH-DME formulation, high Li cycling CE (99.5%) and oxidative stability (6 V) are achieved with a much reduced Li cycling overpotential. A 20 μm Li||NMC532 coin cell lasts 250 cycles with 84% capacity retention. A Cu||NMC811 pouch cell achieves 120 cycles before reaching 75% of initial capacity under lean electrolyte condition (≈2.1 μL mAh^{-1}). Molecular dynamics (MD) simulation

H. Wang, W. Huang, Z. Zhang, Prof. Y. Cui
Department of Materials Science and Engineering
Stanford University
Stanford, CA 94305, USA
E-mail: yicui@stanford.edu

Z. Yu, Dr. X. Kong, Dr. D. G. Mackanic, X. Huang, Prof. J. Qin, Prof. Z. Bao
Department of Chemical Engineering
Stanford University
Stanford, CA 94305, USA
E-mail: zbao@stanford.edu

Z. Yu
Department of Chemistry
Stanford University
Stanford, CA 94305, USA

Prof. Y. Cui
Stanford Institute for Materials and Energy Sciences
SLAC National Accelerator Laboratory
Menlo Park, CA 94025, USA

The ORCID identification number(s) for the author(s) of this article can be found under https://doi.org/10.1002/adma.202008619.

DOI: 10.1002/adma.202008619

confirms that Li-ions are solvated by both FDMH and DME with the participation of multiple anions. This enables highly inorganic, anion-derived SEI with accumulated LiF on the electrode surface, verified through cryogenic transmission electron microscopy (Cryo-TEM) and X-ray photoelectron spectroscopy (XPS). This strategy combining rationally designed high stability molecules with optimized portion of low molecular weight co-solvent benefiting rate capability enables further improved Li-metal battery performances, and will guide further efforts on the electrolyte innovations.

2. Results

2.1. FDMB Analog Molecules as Electrolyte Solvents

To further enhance the molecular stability, we add more -CF_2- groups into the backbone of FDMB. This results in a series of FDMB analog molecules (**Figure 1**a), including fluorinated 1,5-dimethoxypentane (FDMP), fluorinated 1,6-dimethoxyhexane (FDMH), and fluorinated 1,8-dimethoxyoctane (FDMO). These analog molecules maintain LiFSI solubility, resulting in brownish electrolyte colors (Figure 1b). This indicates similar solvation environments as FDMB, with both O and F atoms coordinating with the Li-ions.[31] Linear sweep voltammetry (LSV) confirms that with longer fluorinated backbones, the FDMB analog molecules enable even better oxidative stability (Figure S1, Supporting Information). However, the increased number of -CF_2- groups also leads to reduced salt solubility. 0.7 M LiFSI can be dissolved in FDMP while saturation is reached after 0.15 and 0.05 M LiFSI are dissolved in FDMH and FDMO, respectively (Figure 1b). As a result, electrolytes with these analog molecules as the only solvents show at least doubled impedance (Figure S2, Supporting Information) and Li cycling overpotential (Figure 1c) in Li||Li symmetric cells compared to 1 M LiFSI/FDMB, hindering practical applications.

DME is chosen as a co-solvent to mitigate the above issue, which is compatible with fluorinated ether molecules and has high LiFSI solubility.[19,23,24] However, electrolyte formulation needs to be rationally optimized. On one hand, less -CF_2- in the backbone and higher DME ratio may be beneficial to Li deposition kinetics. On the other hand, more -CF_2- in the backbone and lower DME ratio may improve electrolyte stability toward Li-metal anodes and high-voltage cathodes (Figure 1d). To achieve the optimum formulation, Cu||NMC532 anode-free coin cells are used for the electrolyte screening. Cells are cycled with 5 μL mAh^{-1} of various electrolyte formulations to examine their performances toward both the Li metal and the NMC cathode under practical conditions. It is worth noting that neither increase of fluorination nor too high content of fluorinated molecule leads to continuous performance improvement (Figure 1e,f), which is probably due to the weakened ion conduction and thus fluctuated CE during initial cycling when the overall fluorine content is too high. By tuning either the backbone length or the DME ratio, 1 M LiFSI/6FDMH-DME shows the longest anode-free cycle life (Figure 1e,f), and is selected as the optimized electrolyte formulation for further testing and characterizations.

2.2. Electrochemical Properties

Li-metal CE is first measured for the 1 M LiFSI/6FDMH-DME electrolyte. An average CE of 99.4% is achieved in Li||Cu half-cell cycling (**Figure 2**a) and a CE of 99.5% is achieved following the Aurbach method[32] (Figure 2b). Oxidative stability is tested by LSV of Li||Al cells. Cell using 1 M LiFSI/6FDMH-DME electrolyte shows negligible current under ≈6 V (Figure 2c), which will further promote the high-voltage stability compared to previously reported 1 M LiFSI/FDMB system.[31] These results confirm that the optimized portion of DME does not compromise the excellent stability toward Li-metal anodes and high voltages enabled by the FDMH molecule. Meanwhile, using DME as a co-solvent significantly reduces the Li||Li symmetric cell impedance (Figure 2d). It is found that impedance curve of the Li||Li cell using 1 M LiFSI/6FDMH-DME shows much reduced intercept and semi-circle diameter, indicating lower ionic and interfacial resistance than the cell with 1 M LiFSI/FDMB electrolyte. This facilitates a consistently lower Li cycling overpotential in Li||Li symmetric cells even after long-term cycling (Figure 2e,f) and potentially improved full-cell kinetics.

2.3. Full-Cell Cycling Performances

With the improved Li cycling kinetics, 1 M LiFSI/6FDMH-DME enables good rate capability in Li||NMC532 full cells (**Figure 3**a,b). Over 80% charging/discharging capacity is maintained under 1 C charging or discharging rates (2.7 mA cm^{-2}). Meanwhile, the above-mentioned high Li CE and high voltage stability enables long cycling Li-metal batteries with various configurations. Using 1 M LiFSI/6FDMH-DME electrolyte, a 20 μm Li||NMC532 coin cell (negative/positive capacity ratio, N/P ratio = 1.6) retains 84% of its initial discharge capacity after 250 cycles (Figure 3c), and a 20 μm Li||NMC811 coin cell (N/P ratio = 2) achieves 76% capacity retention after 250 cycles (Figure 3d). Repeated cells show consistent and reproducible cycling results as well (Figure S3, Supporting Information). Meanwhile, 20 μm Li||NMC622 (N/P ratio = 1.3) and 20 μm Li||NMC811 (N/P ratio = 0.8) coin cells last 120 cycles with 78% and 70% capacity retention, respectively (Figure S4, Supporting Information). The 1 M LiFSI/6FDMH-DME electrolyte is also tested in practical anode-free pouch cells. Under ≈2.1 μL mAh^{-1} lean electrolyte condition, Cu||NMC811 pouch cells last 120 cycles before reaching 75% of initial capacity (Figure 3e and Figure S3, Supporting Information). After 121st charging, the cell is disassembled and both electrodes are examined. Surface of the Cu foil shows silverish color (Figure S5a, Supporting Information), indicating uniform Li deposition morphology even after long-term cycling, which is further confirmed through scanning electron microscopy (SEM) imaging (Figure S5b,c, Supporting Information). Cryo-TEM is used to characterize the NMC cathode. Well maintained {003} and {104} crystalline domains of the NMC811 particle are observed without any visible interfacial layer (Figure S6, Supporting Information), further proving the long-term stability of 1 M LiFSI/6FDMH-DME toward high voltage cathodes. Meanwhile, a Cu||NMC532 pouch cell achieves 100 cycles with 70% capacity retention (Figure S7, Supporting Information), and

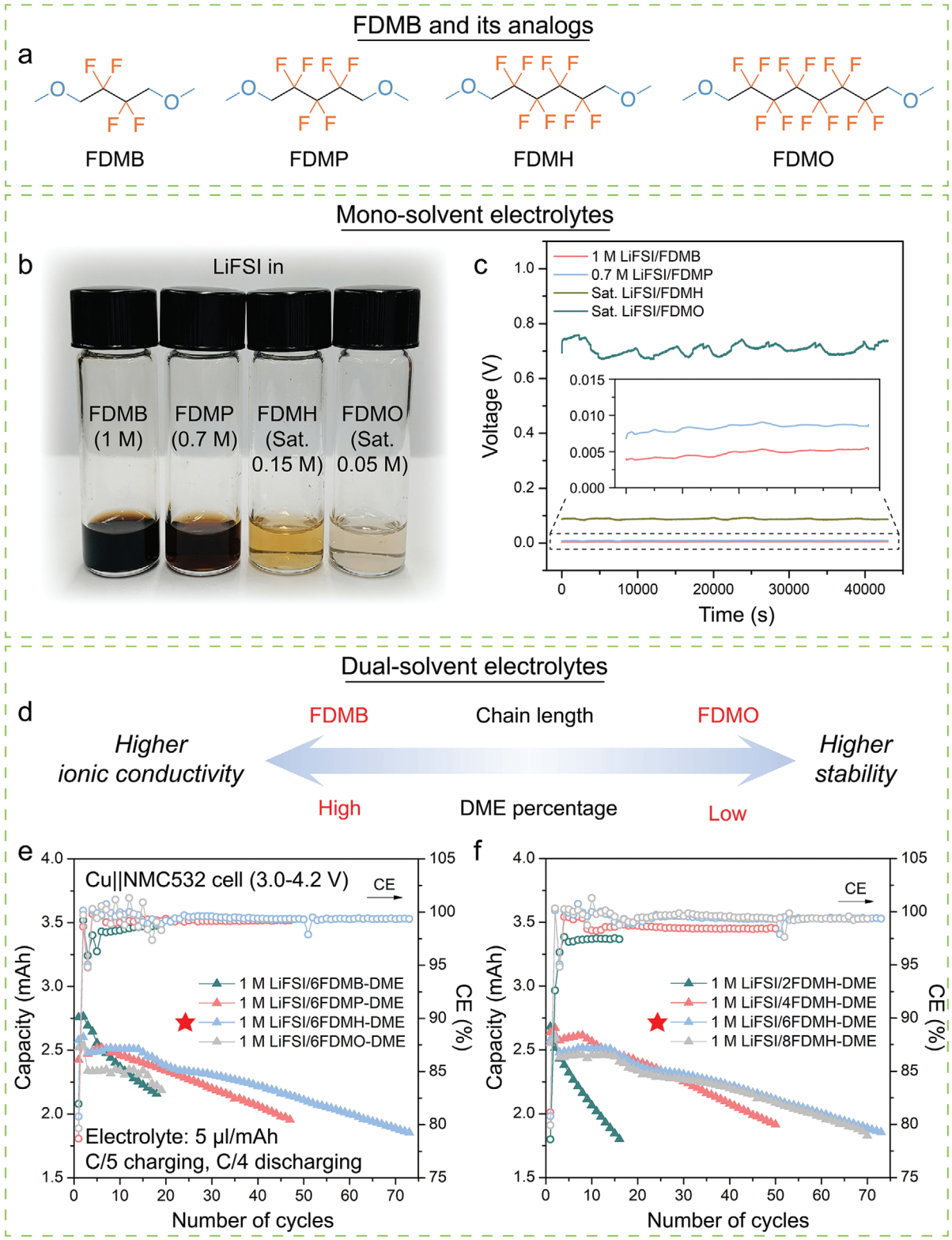

Figure 1. FDMB analog molecules and electrolyte formulation screening. a) Molecular structures of FDMB and its analog molecules FDMP, FDMH, and FDMO. b) Digital photo of electrolytes with LiFSI dissolved in FDMB, FDMP, FDMH, and FDMO. c) Voltage profiles of a Li||Li symmetric cells under 10 µA cm^{-2} current density with different electrolytes. d) Diagram of the design strategy for dual-solvent electrolytes using DME as the co-solvent. e) Cu||NMC532 anode-free cell cycle performances using electrolytes with different fluorinated molecules. f) Cu||NMC532 anode-free cell cycle performances using electrolytes with different FDMH to DME ratios. 1 M LiFSI/6FDMH-DME shows the best performance among all formulations.

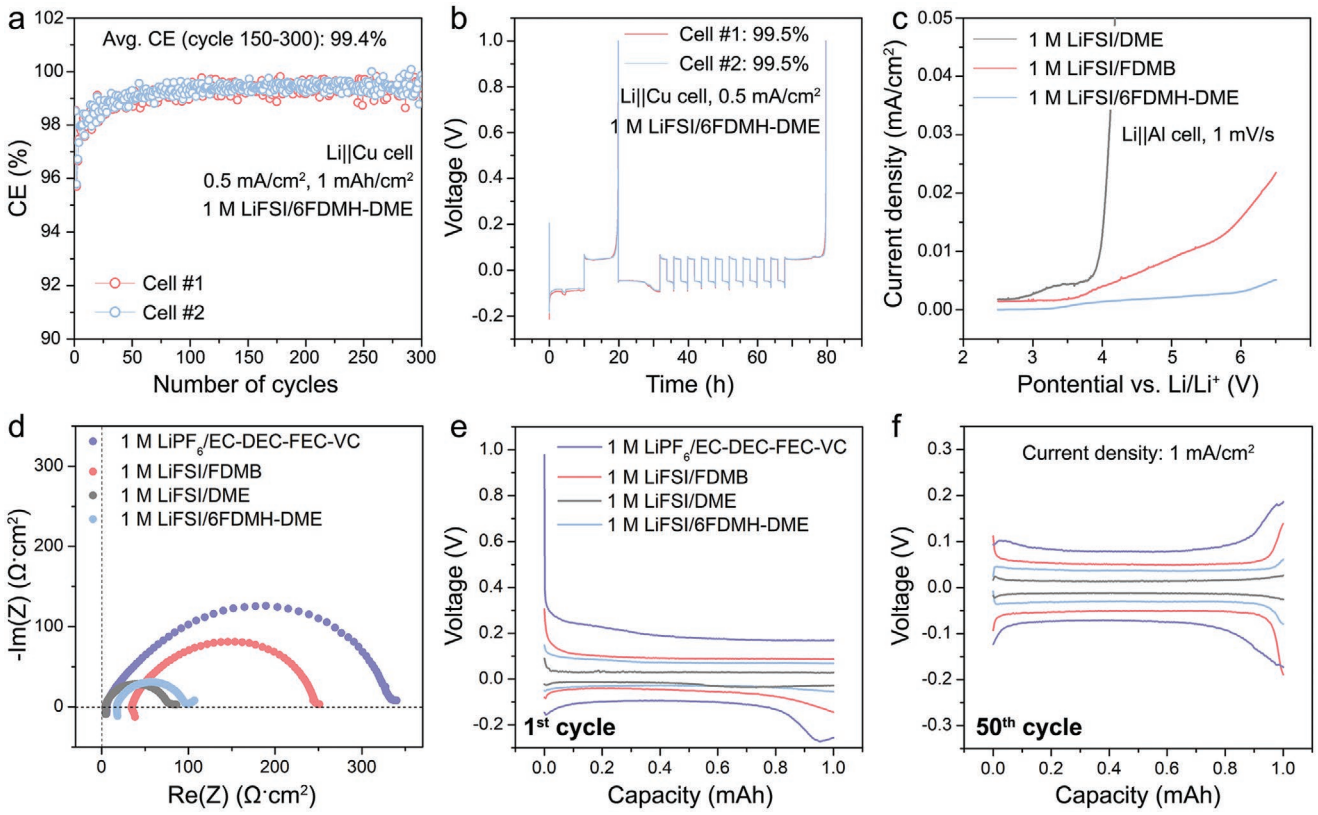

Figure 2. Electrochemical performances of the 1 M LiFSI/6FDMH-DME electrolyte. a) Cycling CE of Li||Cu cells. b) Aurbach CE[32] of Li||Cu cells. c) Oxidative stability characterized by LSV for Li||Al cells. d) Impedance of Li||Li symmetric cells. e) First cycle voltage profile of Li||Li symmetric cells. f) 50th cycle voltage profile of Li||Li symmetric cells. 30 µL of electrolytes are used in all the cells.

a Cu||NMC622 pouch cells lasts 110 cycles with 73% capacity retention (Figure S8, Supporting Information). These data confirm that 1 M LiFSI/6FDMH-DME enables the state-of-the-art Li-metal/anode-free battery performances compared to recent reports (Tables S1 and S2, Supporting Information). Furthermore, the voltage profiles of anode-free cells are studied. After long-term cycling, a cell using 1 M LiFSI/FDMB shows much higher charging/discharging overpotential (Figure S9b, Supporting Information). In contrast, the overpotential of a cell using 1 M LiFSI/6FDMH changes minimally (Figure S9a, Supporting Information). This demonstrates 1 M LiFSI/6FDMH-DME as a promising electrolyte for the long-term stable cycling of Li-metal batteries.

2.4. Li Deposition Morphology and SEI Chemistry

We attribute the high Li-metal cycling performance to the improved Li deposition morphology and the special SEI chemistry in the 1 M LiFSI/6FDMH-DME electrolyte. SEM is first used to characterize the Li deposition morphology. Nonuniform Li deposition are observed in two electrolytes, 1 M lithium hexafluorophosphate ($LiPF_6$)/ethylene carbonate (EC)-diethylene carbonate (DEC)-fluoroethylene carbonate (FEC)-vinylene carbonate (VC) electrolyte and 1 M LiFSI/DME electrolyte (**Figure 4**a,b). In contrast, the deposited Li forms large granules (5–10 µm) in the 1 M LiFSI/6FDMH-DME electrolyte (Figure 4d), resembling the morphology in previously reported 1 M LiFSI/FDMB electrolyte (Figure 4c). The significantly reduced surface area and tortuosity of the deposited Li help to minimize SEI and "dead" Li formation, leading to high cycling efficiency.[33]

Cryo-TEM is used to characterize the compact SEI on the Li surface in the 1 M LiFSI/6FDMH-DME electrolyte. Figure 4e shows a low magnification image of the Li deposited on the Cu grid. Filamentary Li is observed due to the high current density and low capacity deposited during the sample preparation. Selected-area electron diffraction (SAED) pattern (Figure 4f) shows the absence of crystalline domains other than metallic Li, indicating the amorphous nature of the compact SEI. This is further proved by a high-resolution image (Figure 4g). An ≈15 nm layer of fully amorphous compact SEI is observed on the Li surface. Although this compact SEI is slightly thicker than that in previously reported 1 M LiFSI/FDMB,[31] it is structurally similar to those in ether-based electrolytes[23] and still significantly thinner than those in carbonate electrolytes.[34,35] Only Li {110} lattice can be observed in both the TEM image and its fast Fourier transform result (inset of Figure 4g). Chemical composition of the SEI is characterized through energy dispersive X-ray spectroscopy (EDS; Figure 4h). The result shows elements O, F, S, and N are enriched and implies an inorganic SEI with similar chemical compositions as the FSI^- anion.[31]

The SEI chemistry is further characterized through XPS. Three samples are tested and compared. Sample #1 is a Li foil

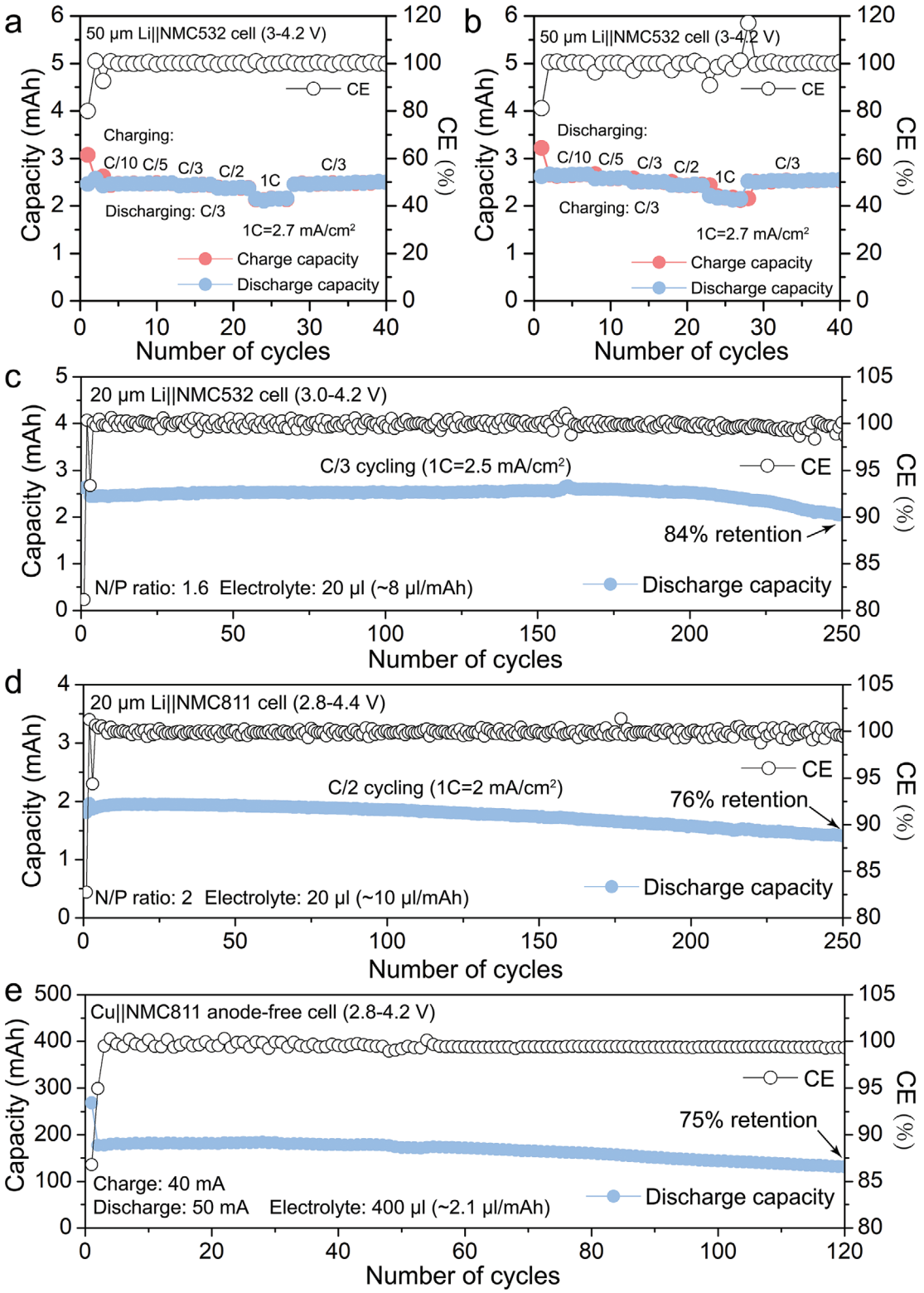

Figure 3. Full cell cycling performances of the 1 M LiFSI/6FDMH-DME electrolyte. a) Rate capability of a Li||NMC532 cell under different charging rates. b) Rate capability of a Li||NMR532 cell under different discharging rates. c) A 20 μm Li||NMC532 coin cell achieves 250 cycles before reaching 84% of initial discharging capacity. d) A 20 μm Li||NMC811 coin cells achieve 250 cycles before reaching 76% of initial discharging capacity. e) A Cu||NMC811 anode-free pouch cell achieves 120 cycles before reaching 75% of initial discharging capacity under lean electrolyte condition (the first cycle was cycled at C/10 rate between 2.8 and 4.4 V).

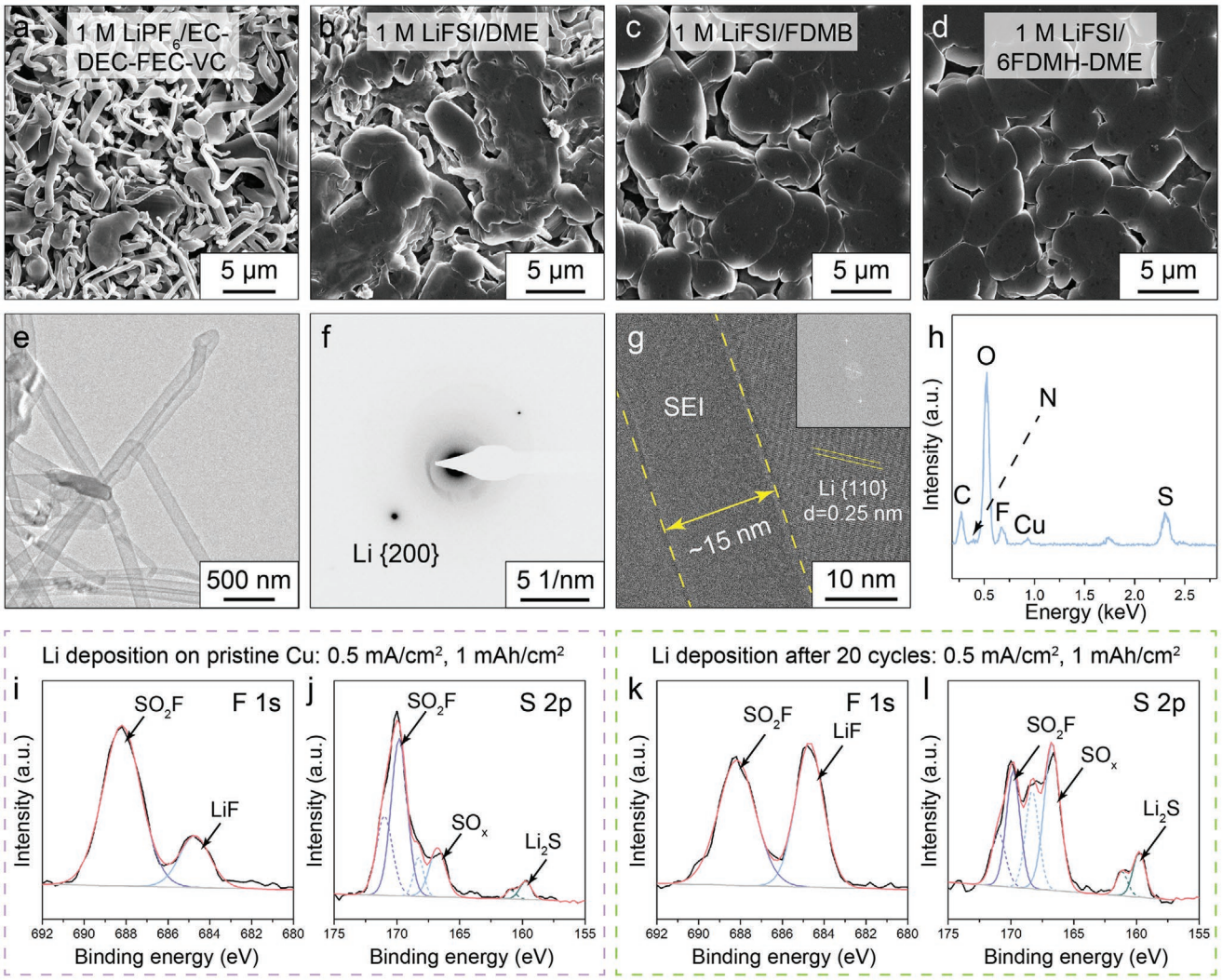

Figure 4. Characterizations on the Li metal deposited in the 1 M LiFSI/6FDMH-DME electrolyte. a–d) SEM images on the morphologies of Li metal deposited in 1 M $LiPF_6$/EC-DEC-FEC-VC (a), 1 M LiFSI/DME (b), 1 M LiFSI/FDMB (c), and 1 M LiFSI/6FDMH-DME (d) under 0.5 mA cm^{-2} and 1 mAh cm^{-2}. e) Cryo-TEM image, f) SAED pattern, g) high-resolution Cryo-TEM image with fast Fourier transform result as the inset and h) EDS mapping of the Li metal deposited in the 1 M LiFSI/6FDMH-DME electrolyte. i) XPS F 1s, j) S 2p spectra of the Li deposited on pristine Cu foil, and k) F 1s, l) S 2p spectra of the Li deposited on a Cu foil after 20 cycles in the 1 M LiFSI/6FDMH-DME electrolyte. For clarity, intermediate species (e.g., SO_xF_y and Li_2S_x) are not labeled.

soaked in 1 M LiFSI/6FDMH-DME for 7 days. Sample #2 is Li deposited on a pristine Cu foil in 1 M LiFSI/6FDMH-DME under 0.5 mA cm^{-2} and 1 mAh cm^{-2}. Sample #3 is Li deposited onto a Cu foil within a Cu||Li cell after 20 cycles (0.5 mA cm^{-2} and 1 mAh cm^{-2} of Li is deposited and stripped until 1 V in each cycle). For sample #1, O, F, S, and N 1s are all observed to resemble the corresponding peaks for the FSI^- anion (Figure S10a–e, Supporting Information). This indicates that the chemically formed SEI is almost fully composed of FSI^- anion decomposition products. For sample #2, the surface is still rich in FSI^- analog species, but small signals from LiF, Li_2S, and Li_2O can be observed (Figure 4i,j and Figure S10f–h, Supporting Information). These new signals further intensify in sample #3 (Figure 4k,l and Figure S10i–k, Supporting Information). Taken together, these results suggest that the FSI^--anion-derived species tend to further decompose electrochemically, resulting in accumulating inorganic LiF, Li_2S, and Li_2O on the electrode surface after continuous cycling. Anion-derived SEI components and LiF have both been observed to improve Li deposition morphology and cycling CE,[19,23,34,36–39] so we believe the SEI chemistry also serves a crucial role for the long cycling of Li-metal anodes in the 1 M LiFSI/6FDMH-DME electrolyte.

2.5. Dual-Solvent Solvation Environment

The Li deposition morphology and SEI chemistry correlate strongly to the Li-ion solvation structures in the electrolyte.[19,35] Therefore, we study the Li-ion solvation in the 1 M LiFSI/6FDMH-DME electrolyte. The 1 M LiFSI/6FDMH-DME resembles recently developed LHCE in its formulation, but the solvation mechanism is distinct. In LHCEs, the fluorinated

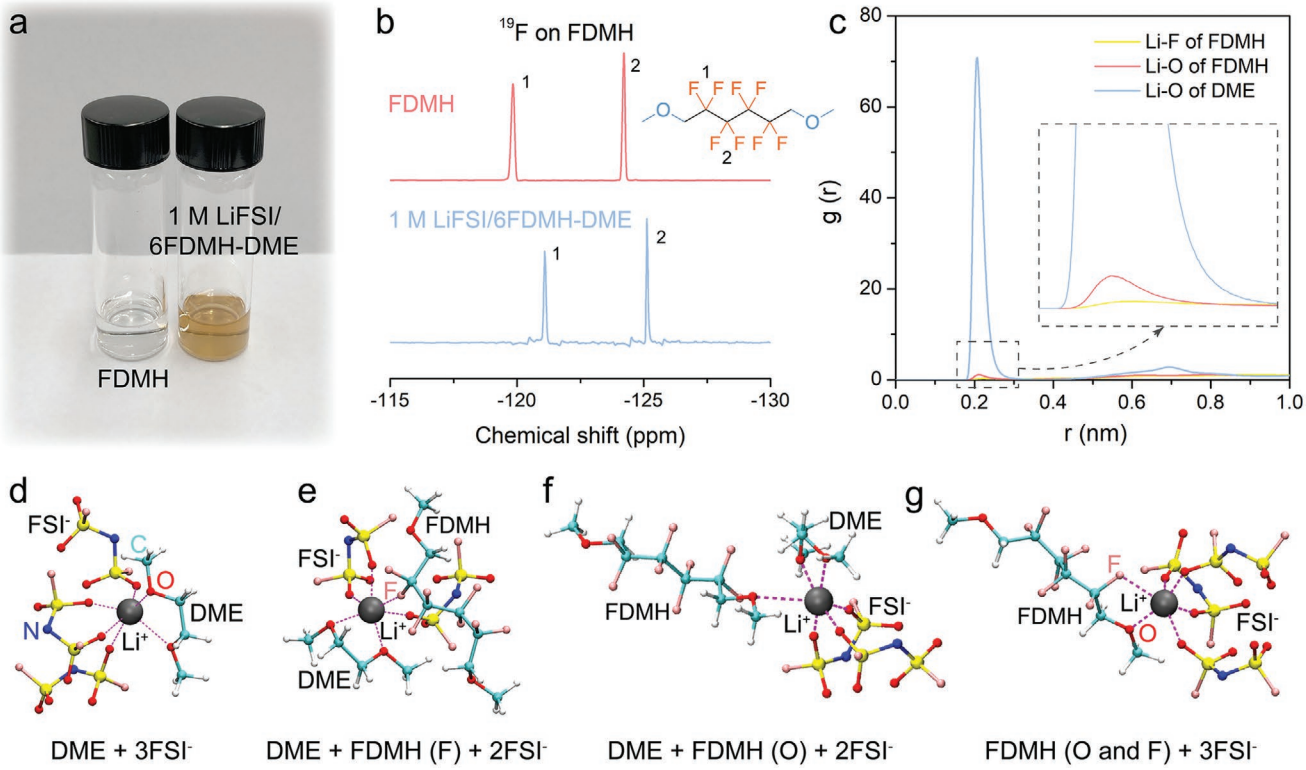

Figure 5. Solvation of Li-ions in the 1 M LiFSI/6FDMH-DME electrolyte. a) Digital photo of pure FDMH and 1 M LiFSI/6FDMH-DME electrolyte. The color of the electrolyte indicates that FDMH participates in the Li-ion solvation. b) ^{19}F NMR of FDMH and 1 M LiFSI/6FDMH-DME. An upfield shift in the ^{19}F peak indicates interactions between Li-ions and F_{FDMH}. c) Radial distribution functions of FDMH and DME molecules around Li-ions in the 1 M LiFSI/6FDMH-DME electrolyte. d–g) Different types of Li-ion solvation environments in the 1 M LiFSI/6FDMH-DME electrolyte through MD simulation. Participation of the O_{FDMH} and F_{FDMH} in the Li-ion solvation can be clearly observed.

molecules serve as diluent and do not participate in the solvation of Li-ions.[18,23,24] In contrast, FDMH and DME both participate in the Li-ion solvation in the 1 M LiFSI/6FDMH-DME electrolyte. First, the 1 M LiFSI/6FDMH-DME electrolyte shows a brownish color (**Figure 5**a), resulting from the interaction between the Li-ions and the F atoms on FDMB and its analog molecules.[31] This indicates F_{FDMH} does coordinate with Li-ions in the 1 M LiFSI/6FDMH-DME electrolyte. Second, ^{19}F NMR peaks show obvious upfield shifts in the 1 M LiFSI/6FDMH-DME electrolyte than pure FDMH (Figure 5b), further verifying the interaction between F_{FDMH} and Li-ions. When FDMH is interacting with Li-ions and participating in the solvation sheath, the surrounding FSI^- anions which are originally in the solvation structure can shield the FDMH molecule, leading to an upfield ^{19}F shift.[24,31] Finally, by using the atomistic MD simulations to resolve the solvation environments in the 1 M LiFSI/6FDMH-DME electrolyte, we find from the radial distribution functions that Li-ions are not only solvated by DME molecules, but also by both O_{FDMH} and F_{FDMH} in the first solvation shell (Figure 5c). This is intrinsically different from previous simulation results for the LHCE systems, where the fluorinated ether molecules do not appear in the Li-ion vicinities.[18] To provide further evidence, several typical Li-ion solvation structures are illustrated in the 1 M LiFSI/6FDMH-DME electrolyte (Figure 5d–g). When only one solvent molecule participates, either two O_{DME} (Figure 5d) or O_{FDMH} and F_{FDMH} (Figure 5g) chelate onto a Li-ion, and three FSI^- anions are incorporated. In other cases, either O_{FDMH} or F_{FDMH} coordinates with a Li-ion, together with O_{DME} and two FSI^- anions (Figure 5e,f). Therefore, these Li-ion solvation structures incorporate both the stable FDMH molecule and multiple anions. This leads to the formation of a highly inorganic, anion-derived SEI (Figure 4h–l), which is critical to the improved Li deposition morphology and Li metal battery cycling performances demonstrated above.

3. Conclusion

We propose a new design strategy for Li-metal battery electrolytes. FDMH molecule is used as the main solvent to promote electrolyte stability. DME is used as the co-solvent to reduce ionic and interfacial resistance. After rational formulation optimization, the 1 M LiFSI/6FDMH-DME electrolyte enables 99.5% Li cycling CE and 6 V oxidative stability with a much reduced Li cycling overpotential and much improved rate capability. Furthermore, a 20 μm Li‖NMC532 coin cell lasts 250 cycles with 84% capacity retention and a Cu‖NMC811 pouch cell achieves 120 cycles with 75% capacity retention under lean electrolyte condition (≈2.1 μL mAh^{-1}). These state-of-the-art Li-metal battery performances are attributed to a low surface area Li deposition morphology and inorganic, anion-derived

SEI with accumulated LiF on the electrode surface. With MD simulation, we show that this is enabled by the specific Li-ion solvation environments where the stable FDMH molecules and multiple FSI^- anions coordinate with the Li-ions. This design of dual-solvent Li-ion solvation will possibly inspire a series of new electrolyte formulations for long-cycling Li-metal batteries in the future.

4. Experimental Section

Materials: 2,2,3,3-Tetrafluoro-1,4-butanediol, 2,2,3,3,4,4-hexafluoro-1,5-pentanediol, 2,2,3,3,4,4,5,5-octafluoro-1,6-hexanediol, 1*H*,1*H*,8*H*,8*H*-dodecafluoro-1,8-octanediol were purchased from Synquest Lab. Methyl iodide, sodium hydride (60% in mineral oil) and other general reagents were purchased from Sigma Aldrich or Fisher Scientific. All chemicals were used without further purification. LiFSI was purchased from Fluolyte; VC and FEC were purchased from Sigma-Aldrich. DME (99.5% over molecular sieves) was purchased from Acros. 1 M $LiPF_6$ in EC/DEC (LP40) was purchased from Gotion. The commercial Li-battery separator Celgard 2325 (25 µm thick, polypropylene/polyethylene/polypropylene) was purchased from Celgard and used in all coin cells and pouch cells. Cu current collector (25 µm thick) was purchased from Alfa Aesar. Thin Li foils (20 µm) were provided by Hydro-Québec. NMC532 cathode sheets were purchased from MTI (2 mAh cm^{-2}), and NMC811 cathode sheets were purchased from Targray (2 mAh cm^{-2} (10.02 mg cm^{-2}) and 4.5 mAh cm^{-2} (20.47 mg cm^{-2})). Other battery materials, such as 2032-type coin-cell cases, springs, and spacers, were all purchased from MTI.

Synthesis: FDMB and FDMP were synthesized with the same procedure as the previous report.[31]

FDMH was synthesized by one-step methylation (Figures S11–S14, Supporting Information): to a round-bottom flask were added dry tetrahydrofuran and 2,2,3,3,4,4,5,5-octafluoro-1,6-hexanediol. The solution was cooled to 0 °C and then 2.5 equivalents of NaH were added slowly. Bubbling was observed upon NaH addition. Then, 2.5 equivalents of MeI were added dropwise to the stirring suspension. The suspension was stirred at room temperature for 2 h and then heated to reflux for overnight. The mixture was then filtered off and the solvents were removed under vacuo. The crude product was vacuum distilled to yield the final product as colorless liquid. The product was then filtered off through 0.45 µm polytetrafluoroethylene filter and transferred to an argon glovebox for further use. Yield: ≈70%. ^{1}H NMR (400 MHz, d^6-DMSO, δ/ppm): 4.03–3.95 (t, 4H), 3.41 (s, 6H). ^{13}C NMR (100 MHz, d^6-DMSO, δ/ppm): 116.51–108.99, 69.15–68.65, 60.29. ^{19}F NMR (376 MHz, d^6-DMSO, δ/ppm): –119.83 (s, 4F), –124.21 (s, 4F).

FDMO was synthesized by similar procedure to that of FDMH, except the reactant was changed to 1*H*,1*H*,8*H*,8*H*-dodecafluoro-1,8-octanediol (Figures S15–S18, Supporting Information). Yield: ≈75%. ^{1}H NMR (400 MHz, $CDCl_3$, δ/ppm): 3.91–3.84 (t, 4H), 3.51 (s, 6H). ^{13}C NMR (100 MHz, $CDCl_3$, δ/ppm): 116.15–108.72, 69.82–69.32, 60.78. ^{19}F NMR (376 MHz, $CDCl_3$, δ/ppm): –120.28 (s, 4F), –122.70 (s, 4F), –124.19 (s, 4F).

After the syntheses, corresponding electrolytes were made and stored in the argon glovebox. The densities for all these electrolytes were measured to be ≈1.25 g mL^{-1}.

MD Simulations: Molecules and ions were described by the optimized potentials for a liquid simulations all-atom (OPLS-AA) force field.[40] The simulation box was composed of 356 FDMH, 117 DME, and 85 pairs of LiFSI. During simulations, the temperature was controlled at 300 K using a Nosé–Hoover thermostat with a relaxation time of 0.2 ps and the pressure was controlled at 1 bar using a Parrinello–Rahman barostat with a relaxation time of 2.0 ps. All MD simulations were conducted with the GROMACS 2018 program[41] for 50 ns, and the last 40 ns were used for analysis. Li-ion solvation structures were analyzed with a self-written script based on the MDAnalysis Python module.[42]

Characterizations: NMR spectra were recorded on a Varian Mercury 400-MHz NMR spectrometer at room temperature. An FEI Titan 80–300 environmental (scanning) transmission electron microscope and a Gatan 626 holder were used for Cryo-TEM experiments. Cryo-TEM sample preparations prevent air reaction and beam damage, as described previously.[35] Low-dose electron exposure procedures were employed using a Gatan K3 IS direct electron detector camera, enabling Cryo-HRTEM with an electron dose of <100 e^- $Å^{-2}$. The TEM is equipped with an aberration corrector in the image-forming lens, which was tuned before imaging. An FEI Magellan 400 XHR SEM was used for SEM characterizations. XPS profiles were collected with a PHI VersaProbe 1 scanning XPS microprobe. All Li-metal samples were rinsed thoroughly with pure FDMH and dried inside an argon-filled glovebox before characterizations.

Electrochemical Measurements: Electrochemical impedance spectroscopy, LSV, and pouch-cell cycling were carried out on a Biologic VMP3 system. The cycling tests for coin cells were carried out on an Arbin system. The electrochemical impedance spectroscopy measurements were taken over a frequency range of 7 MHz to 100 mHz. For Li||Cu half-cell CE cycling tests, cycling was done by depositing 1 mAh cm^{-2} of Li onto the Cu electrode followed by stripping to 1 V. For the Aurbach CE test,[32] a standard protocol was followed: 1) performed one initial formation cycle with Li deposition of 5 mAh cm^{-2} on Cu under 0.5 mA cm^{-2} and stripping to 1 V; 2) deposited 5 mAh cm^{-2} Li on Cu under 0.5 mA cm^{-2} as a Li reservoir; 3) repeatedly stripped/deposited Li of 1 mAh cm^{-2} under 0.5 mA cm^{-2} for 10 cycles; 4) stripped all Li to 1 V. The Li||NMC and Cu||NMC full-cells were cycled with the following method: after the first one or two formation cycles at C/10 charge/discharge, the cells were cycled at different rates. Then a constant-current–constant-voltage protocol was used for cycling: cells were charged to top voltage and then held at that voltage until the current dropped below C/20. All cells were cycled under ambient conditions without temperature control.

Acknowledgements

This work was supported by the U.S. Department of Energy, under the Assistant Secretary for Energy Efficiency and Renewable Energy, Office of Vehicle Technologies, the Battery Materials Research (BMR) Program, and Battery 500 Consortium. Part of this work was performed at the Stanford Nano Shared Facilities (SNSF), supported by the National Science Foundation under award ECCS-1542152. K3 IS camera and support are courtesy of Gatan. All authors thank K. Zaghib from Hydro-Québec for preparing and providing the thin Li metal foils.

Conflict of Interest

This work has been filed as US Provisional Patent Application No. 62/928,638.

Author Contributions

H.W. and Z.Y. contributed equally to this work. H.W., Z.Y., Z.B., and Y.C. conceived the project and designed the experiments. H.W. carried out electrolyte screening, battery fabrication, and testing, as well as XPS characterizations. Z.Y. synthesized FDMB analog molecules and helped with battery testing. X.K. performed MD simulations. W.H. and Z.Z. performed SEM and Cryo-TEM characterizations. D.M performed NMR characterizations. X.H. helped with chemical synthesis. H.W., Z.Y., Z.B., and Y.C. co-wrote the manuscript, with input from all authors.

Data Availability Statement

The data that support the findings of this study are available from the corresponding author upon reasonable request.

Keywords

anode-free batteries, Coulombic efficiency, electrolytes, fluorinated solvents, Li-metal batteries

Received: December 21, 2020
Revised: February 3, 2021
Published online:

[1] D. Lin, Y. Liu, Y. Cui, *Nat. Nanotechnol.* **2017**, *12*, 194.
[2] H. Wang, Y. Liu, Y. Li, Y. Cui, *Electrochem. Energy Rev.* **2019**, *2*, 509.
[3] Z. Yu, Y. Cui, Z. Bao, *Cell Rep. Phys. Sci.* **2020**, *1*, 100119.
[4] G. Zheng, S. W. Lee, Z. Liang, H.-W. Lee, K. Yan, H. Yao, H. Wang, W. Li, S. Chu, Y. Cui, *Nat. Nanotechnol.* **2014**, *9*, 618.
[5] H. Chen, A. Pei, D. Lin, J. Xie, A. Yang, J. Xu, K. Lin, J. Wang, H. Wang, F. Shi, D. Boyle, Y. Cui, *Adv. Energy Mater.* **2019**, *9*, 1900858.
[6] Z. Yu, D. G. Mackanic, W. Michaels, M. Lee, A. Pei, D. Feng, Q. Zhang, Y. Tsao, C. V. Amanchukwu, X. Yan, H. Wang, S. Chen, K. Liu, J. Kang, J. Qin, Y. Cui, Z. Bao, *Joule* **2019**, *3*, 2761.
[7] Y.-T. Weng, H.-W. Liu, A. Pei, F. Shi, H. Wang, C.-Y. Lin, S.-S. Huang, L.-Y. Su, J.-P. Hsu, C.-C. Fang, Y. Cui, N.-L. Wu, *Nat. Commun.* **2019**, *10*, 5824.
[8] S. T. Oyakhire, W. Huang, H. Wang, D. T. Boyle, J. R. Schneider, C. de Paula, Y. Wu, Y. Cui, S. F. Bent, *Adv. Energy Mater.* **2020**, *10*, 2002736.
[9] Y. Gao, T. Rojas, K. Wang, S. Liu, D. Wang, T. Chen, H. Wang, A. T. Ngo, D. Wang, *Nat. Energy* **2020**, *5*, 534.
[10] K. Yan, Z. Lu, H.-W. Lee, F. Xiong, P.-C. Hsu, Y. Li, J. Zhao, S. Chu, Y. Cui, *Nat. Energy* **2016**, *1*, 16010.
[11] D. Lin, Y. Liu, Z. Liang, H.-W. Lee, J. Sun, H. Wang, K. Yan, J. Xie, Y. Cui, *Nat. Nanotechnol.* **2016**, *11*, 626.
[12] H. Wang, D. Lin, Y. Liu, Y. Li, Y. Cui, *Sci. Adv.* **2017**, *3*, e1701301.
[13] H. Wang, Y. Li, Y. Li, Y. Liu, D. Lin, C. Zhu, G. Chen, A. Yang, K. Yan, H. Chen, Y. Zhu, J. Li, J. Xie, J. Xu, Z. Zhang, R. Vilá, A. Pei, K. Wang, Y. Cui, *Nano Lett.* **2019**, *19*, 1326.
[14] H. Wang, D. Lin, J. Xie, Y. Liu, H. Chen, Y. Li, J. Xu, G. Zhou, Z. Zhang, A. Pei, Y. Zhu, K. Liu, K. Wang, Y. Cui, *Adv. Energy Mater.* **2019**, *9*, 1802720.
[15] Z. Liang, K. Yan, G. Zhou, A. Pei, J. Zhao, Y. Sun, J. Xie, Y. Li, F. Shi, Y. Liu, D. Lin, K. Liu, H. Wang, H. Wang, Y. Lu, Y. Cui, *Sci. Adv.* **2019**, *5*, eaau5655.
[16] H. Chen, A. Pei, J. Wan, D. Lin, R. Vilá, H. Wang, D. Mackanic, H.-G. Steinrück, W. Huang, Y. Li, A. Yang, J. Xie, Y. Wu, H. Wang, Y. Cui, *Joule* **2020**, *4*, 938.
[17] H. Wang, X. Cao, H. Gu, Y. Liu, Y. Li, Z. Zhang, W. Huang, H. Wang, J. Wang, W. Xu, J.-G. Zhang, Y. Cui, *ACS Nano* **2020**, *14*, 4601.
[18] S. Chen, J. Zheng, D. Mei, K. S. Han, M. H. Engelhard, W. Zhao, W. Xu, J. Liu, J.-G. Zhang, *Adv. Mater.* **2018**, *30*, 1706102.
[19] J. Qian, W. A. Henderson, W. Xu, P. Bhattacharya, M. Engelhard, O. Borodin, J.-G. Zhang, *Nat. Commun.* **2015**, *6*, 6362.
[20] K. Xu, *Chem. Rev.* **2004**, *104*, 4303.
[21] K. Xu, *Chem. Rev.* **2014**, *114*, 11503.
[22] X. Fan, L. Chen, X. Ji, T. Deng, S. Hou, J. Chen, J. Zheng, F. Wang, J. Jiang, K. Xu, C. Wang, *Chem* **2018**, *4*, 174.
[23] X. Cao, X. Ren, L. Zou, M. H. Engelhard, W. Huang, H. Wang, B. E. Matthews, H. Lee, C. Niu, B. W. Arey, Y. Cui, C. Wang, J. Xiao, J. Liu, W. Xu, J.-G. Zhang, *Nat. Energy* **2019**, *4*, 796.
[24] X. Ren, L. Zou, X. Cao, M. H. Engelhard, W. Liu, S. D. Burton, H. Lee, C. Niu, B. E. Matthews, Z. Zhu, C. Wang, B. W. Arey, J. Xiao, J. Liu, J.-G. Zhang, W. Xu, *Joule* **2019**, *3*, 1662.
[25] J. Zheng, M. H. Engelhard, D. Mei, S. Jiao, B. J. Polzin, J.-G. Zhang, W. Xu, *Nat. Energy* **2017**, *2*, 17012.
[26] R. Weber, M. Genovese, A. J. Louli, S. Hames, C. Martin, I. G. Hill, J. R. Dahn, *Nat. Energy* **2019**, *4*, 683.
[27] X. Fan, X. Ji, L. Chen, J. Chen, T. Deng, F. Han, J. Yue, N. Piao, R. Wang, X. Zhou, X. Xiao, L. Chen, C. Wang, *Nat. Energy* **2019**, *4*, 882.
[28] W. Xue, Z. Shi, M. Huang, S. Feng, C. Wang, F. Wang, J. Lopez, B. Qiao, G. Xu, W. Zhang, Y. Dong, R. Gao, Y. Shao-Horn, J. A. Johnson, J. Li, *Energy Environ. Sci.* **2020**, *13*, 212.
[29] C. S. Rustomji, Y. Yang, T. K. Kim, J. Mac, Y. J. Kim, E. Caldwell, H. Chung, Y. S. Meng, *Science* **2017**, *356*, eaal4263.
[30] Y. Yang, D. M. Davies, Y. Yin, O. Borodin, J. Z. Lee, C. Fang, M. Olguin, Y. Zhang, E. S. Sablina, X. Wang, C. S. Rustomji, Y. S. Meng, *Joule* **2019**, *3*, 1986.
[31] Z. Yu, H. Wang, X. Kong, W. Huang, Y. Tsao, D. G. Mackanic, K. Wang, X. Wang, W. Huang, S. Choudhury, Y. Zheng, C. V. Amanchukwu, S. T. Hung, Y. Ma, E. G. Lomeli, J. Qin, Y. Cui, Z. Bao, *Nat. Energy* **2020**, *5*, 526.
[32] B. D. Adams, J. Zheng, X. Ren, W. Xu, J.-G. Zhang, *Adv. Energy Mater.* **2018**, *8*, 1702097.
[33] C. Fang, J. Li, M. Zhang, Y. Zhang, F. Yang, J. Z. Lee, M.-H. Lee, J. Alvarado, M. A. Schroeder, Y. Yang, B. Lu, N. Williams, M. Ceja, L. Yang, M. Cai, J. Gu, K. Xu, X. Wang, Y. S. Meng, *Nature* **2019**, *572*, 511.
[34] W. Huang, H. Wang, D. T. Boyle, Y. Li, Y. Cui, *ACS Energy Lett.* **2020**, *5*, 1128.
[35] Y. Li, Y. Li, A. Pei, K. Yan, Y. Sun, C.-L. Wu, L.-M. Joubert, R. Chin, A. L. Koh, Y. Yu, J. Perrino, B. Butz, S. Chu, Y. Cui, *Science* **2017**, *358*, 506.
[36] X. Fan, L. Chen, O. Borodin, X. Ji, J. Chen, S. Hou, T. Deng, J. Zheng, C. Yang, S.-C. Liou, K. Amine, K. Xu, C. Wang, *Nat. Nanotechnol.* **2018**, *13*, 715.
[37] Y. Lu, Z. Tu, L. A. Archer, *Nat. Mater.* **2014**, *13*, 961.
[38] J. Hu, K. Chen, C. Li, *ACS Appl. Mater. Interfaces* **2018**, *10*, 34322.
[39] C. Li, L. Gu, J. Maier, *Adv. Funct. Mater.* **2012**, *22*, 1145.
[40] W. L. Jorgensen, D. S. Maxwell, J. Tirado-Rives, *J. Am. Chem. Soc.* **1996**, *118*, 11225.
[41] M. J. Abraham, T. Murtola, R. Schulz, S. Páll, J. C. Smith, B. Hess, E. Lindahl, *SoftwareX* **2015**, *1–2*, 19.
[42] N. Michaud-Agrawal, E. J. Denning, T. B. Woolf, O. Beckstein, *J. Comput. Chem.* **2011**, *32*, 2319.